A retrospective study of the pre-eruptive unrest on El Hierro (Canary Islands): implications of seismicity and deformation in the short-term volcanic hazard assessment

Stefania Bartolini[1,a], Carmen López[2], Laura Becerril[1], Rosa Sobradelo[3], Joan Martí[1]

[1] Group of Volcanology, (SIMGEO-UB) CSIC, Institute of Earth Sciences Jaume Almera, c/Lluis Sole Sabaris s/n, 08028 Barcelona, Spain.

[2] Observatorio Geofísico Central, Instituto Geográfico Nacional (IGN), c/Alfonso XII, 3, 28014 Madrid, Spain.

[3] Willis Research Network and Analytics Technology, Willis Towers Watson, London, UK.

[a] Corresponding author: Stefania Bartolini, Group of Volcanology, (SIMGEO-UB) CSIC, Institute of Earth Sciences Jaume Almera, c/Lluis Sole Sabaris s/n, 08028 Barcelona, Spain. (sbartolini.1984@gmail.com)

Key points

· Short-term spatio-temporal analysis for understanding unrest indicators during an unrest phase.

· A new methodology to be applied in short-term hazard assessment.

· Spatio-temporal analysis using information obtained from monitoring data.

Abstract

The correct identification and interpretation of unrest indicators are useful for forecasting volcanic eruptions, delivering early warnings, and understanding the changes occurring in a volcanic system prior to an eruption. Such indicators play an important role in upgrading previous long-term volcanic hazard assessments and help grasp the complexities of the preceding period of eruptive activity. In this work, we present a retrospective analysis of the 2011 unrest episode on the island of El Hierro that preceded a submarine eruption. We use seismic and surface deformation monitoring data to compute the susceptibility analysis (QVAST tool) and to study the evolution over time of the unrest (ST-HASSET tool). Additionally, we show the advantages to be gained by using continuous monitoring data and hazard assessment e-tools to upgrade spatio-temporal analyses and thus visualize more simply the development of the volcanic activity.

Keywords

Short-term volcanic hazard assessment, unrest, precursors, monitoring, spatio-temporal analysis

1. Introduction

The most challenging aspect of forecasting volcanic eruptions is the correct identification and interpretation of precursors during the episodes of unrest that normally precede eruptive activity. During this phase, the short-term volcanic hazard assessment can be computed by combining a long-term hazard analysis with real-time monitoring data, updating continuously the status of the volcanic hazard (Blong, 2000; Sobradelo and Martí, 2015; Tonini et al., 2016). Short-term evaluations can help forecast the likely outcomes – i.e. where and when the eruption will take place – by drawing on the information derived from indicators and an understanding of the volcanic system. The parameters associated with the volcanic process are the geophysical and geochemical signals that provide information on magma movement within the volcanic system and on how the magma is preparing to reach the surface (Chouet, 1996; McNutt, 1996).

In particular, the signals recorded during unrest episodes – for example, an increase in activity compared to the previous background level (Phillipson et al., 2013) – can be used to deduce changes in magma accumulation and movement, the state of stress of the host rock, and the physical and chemical properties of the magma itself (Harrington and Brodsky, 2007; Jellinek and Bercovici, 2011; Lavallée et al., 2008; McNutt, 2005; Neuberg et al., 2000; Papale, 1999; Tárraga et al., 2014). A comprehensive well organized monitoring network on and around the volcano is fundamental if scientists are to analyze how the eruption process is evolving. Changes may be detected on the surface that reflect variations in the geophysical (e.g. seismicity, surface deformation, and changes in potential fields) and/or geochemical (e.g. gas flow rate and gas composition) parameters sensed by the network that is monitoring the

50 activity of the volcano (Scarpa and Tilling, 1996; Sparks, 2003; Vallianatos et al., 2013,
51 Telesca et al., 2015).

52 It is essential that all the monitoring information obtained during an unrest phase
53 be processed and interpreted in real time. This is a crucial consideration since this
54 information is vital in eruption forecasting and provides support for decision-makers. In
55 many instances during an unrest phase, the institution in charge of the monitoring
56 network is expected to publish daily or even hourly bulletins with updates derived from
57 monitoring signals. These bulletins are then used by experts (e.g. a scientific committee
58 or crisis team) to keep public officials abreast of the state of the volcanic system. These
59 reports do not generally contain probabilistic model results and tend to consist merely
60 of processed monitoring data related to seismicity, deformation, and gas emissions.

61 In order to provide a simple and automated way of assessing the evolution of the
62 volcanic system from looking at the monitoring signals, the ST-HASSET was
63 developed (Sobradelo and Martí, 2015; Bartolini et al., 2016). This e-tool offers an
64 alternative to the BET-EF (Marzocchi et al., 2008) and BET-UNREST (Tonini et al.,
65 2016) and also proposes a flexible probabilistic approach to incorporate monitoring
66 information for the quantification of short-term volcanic hazard that looks for
67 significant changes in the values of the measured unrest indicators, across consecutive
68 time intervals. In comparison to the BET-EF and BET-UNREST, ST-HASSET does not
69 focus on the absolute value of each variable with respect to a defined threshold, but
70 compares its degree of change with respect to the previous time interval. In each case, a
71 variation that is considered significant can be defined in advance given the specific
72 characteristics of the volcano being studied.

73 Assuming that the geophysical indicators such as seismicity and ground
74 deformation provide insights on the location of magma during the unrest phase (Endo

and Murray, 1991; Chouet, 1996; McNutt, 1996; Martí et el., 2013), changes in the location of such unrest parameters may indicate magma movement and, consequently, that the location of potential new vents may also change. This is extremely important when conducting hazard assessment analysis, as the location of the eruptive vent may condition the resulting hazards and their potential impacts. In this sense, short-term hazard assessment needs to inform in real time on how monitoring information changes the probabilities of vent opening (volcanic susceptibility) and of the hazards that may occur, as well as of the proximity of the eruptive event.

In order to show how ST-HASSET works, we apply it retrospectively to the unrest episode that preceded the El Hierro eruption in 2011. When volcanic unrest started here in July 2011, the Spanish National Geographical Institute (IGN), the institution responsible for volcano monitoring in Spain, set up a dense seismic monitoring network composed of a three-component (3CC) broadband station (CTIG) and eight short- and medium-period (natural periods of 1 and 5 s) 3CC stations (López et al., 2012) (Fig. 1). In order to monitor the associated 3D deformation, the IGN also deployed four extra GPS stations on El Hierro to reinforce the capacity of the single pre-existing GPS station (FRON) (Fig. 1) belonging to the Canarian Regional government (López et al., 2012, 2014; Martí et al., 2013). The amount of information registered provides a good example of a monitored unrest episode with a complete dataset. However, during the pre-eruptive unrest phase the continuous changes in the position of the seismicity and deformation sources made it all but impossible to forecast the position of the new vent and, consequently, to define reliable eruption scenarios.

The objective of this retrospective analysis is to define guidelines on how we can manage the information generated by a monitoring network during the unrest phase of an ongoing crisis. We use the data recorded in the pre-eruptive unrest episode that

100 took place on El Hierro in 2011 to update in real time the spatial probability of the new
101 vent opening and to interpret the unrest precursors as a means of determining the
102 probability of evolution of these indicators. So, we first evaluate the volcanic
103 susceptibility combining the real time monitoring information with the QVAST tool
104 (Bartolini et al., 2013), which provides a real time variation of the vent opening
105 probabilities. Then, we combine each updated result with the ST-HASSET tool to
106 determine the evolution over time of the unrest indicators. The results obtained allow us
107 to realise how the application of these tools helps interpret the unrest indicators and how
108 they can be used for improving the susceptibility assessment and the definition of
109 realistic eruptive scenarios, thus facilitating the decision making process and the
110 management of the volcanic crisis.
111
112 **2. Methodology**
113 The methodology used in this study basically consists in the systematic
114 application of two e-tools specifically designed for conducting probabilistic spatial and
115 temporal analysis in volcanic hazard assessment.
116 QVAST (Bartolini et al., 2013) is a tool that has been developed to evaluate the
117 spatial probability of a new vent opening (volcanic susceptibility) using volcano-
118 structural data and seismicity. In monogenetic volcanism, as it is the case of El Hierro,
119 each new eruption creates a different vent, which indicates that accurate spatial
120 forecasting is highly uncertain. This type of analysis has been often applied in long-term
121 hazard assessment as it represents a good starting point for developing hazard maps
122 based on certain assumptions: i) future eruptive vents will be close to the previous ones
123 and ii) the stress field plays the most significant role in determining where magma will
124 reach the surface (see Martí et al., 2016). The result is a (long-term) susceptibility map

obtained by assigning different weights to each of the probability density functions in each dataset (volcano-structural elements: location of past vents, eruptive fissures, fractures, faults, dykes, etc.) considered in the analysis, which are combined via a weighted sum and modelled in a non-homogeneous Poisson process. During an unrest phase, the (short-term) susceptibility map varies as new information (e.g. the location of the seismic events) is provided by monitoring data. Hence, the previously defined probabilities of hosting a new vent will change in terms of where the new seismicity and/or ground deformation is located — assuming that both parameters provide an indication of magma movement and location.

The probability of occurrence of a possible eruptive scenario will change according to the variations in the short-term susceptibility map, which will be redefined each time that new monitoring information will be computed; thus, we also have to calculate the temporal evolution of monitoring data.

The ST-HASSET tool (Sobradelo and Martí, 2015; Bartolini et al., 2016) is a simple tool that develops an event tree structure that uses a quantitative approach via Bayesian inference to assess the hazard of a particular volcanic scenario by taking into account monitoring data and all relevant data pertaining to the past history of the volcano. Indicators are shown on a common probability scale to visualize their progress during the unrest phase and to estimate the probability of occurrence of a particular eruptive scenario.

3. Unrest on El Hierro in 2011

El Hierro, situated in the southwestern corner of the Canary archipelago (Fig. 1), is geologically the youngest of these islands and its oldest subaerial rocks have been dated at 1.12 Ma (Guillou et al., 1996). It corresponds to a shield structure formed by different

150 volcanic edifices with three rift zones along which recent volcanism has been
151 concentrated (Guillou et al., 1996). The studied unrest period started on 19 July 2011
152 and gave rise to a submarine eruption that started on 10 October 2011 (Fig. 1). The
153 whole episode was well monitored by the IGN and during the period leading up to the
154 eruption approximately 10,000 earthquakes with local magnitudes of up to 4.3 were
155 recorded, and over 5 cm of vertical and horizontal surface deformations were registered
156 (López et al., 2014).

157 This pre-eruptive unrest started with a marked increase in seismicity, followed a
158 few days later by surface deformation and gas emissions (López et al., 2012). The
159 evolution of the seismicity during this episode was characterized by changes in the
160 hypocentral location that were interpreted as movements in the position of the magma
161 (Fig. 2 and Table 1) (López et al., 2012, 2014). During the first weeks of unrest, all the
162 seismic events were located in the north of the island at a depth of about 10–15 km b.s.l.
163 and were of low magnitude. As of 4–26 September 2011, the seismicity migrated
164 southwards along the crust/mantle boundary and the amount of released seismic energy
165 increased. GPS stations translated towards North, suggesting a simultaneous surface
166 deformation pattern that reflected a correlated migration of the pressure source towards
167 the south. From 27 September to 7 October 2011, both the seismic rate and the seismic
168 energy grew and events were now located mostly off the SW coast of El Hierro. At the
169 same time, a sudden deflation–reinflation was observed on the N–S component at all
170 GPS stations (1–5 October 2011). On 8 October at 20:34 h (GMT), a 4.3 ML
171 earthquake (the greatest magnitude recorded during the unrest period) occurred 1.5 km
172 off the SW coast of the island at a depth of 12 km. However, from this moment
173 onwards, very few further earthquakes were registered and the pre-eruptive episode
174 culminated with a submarine eruption on the southern flank of the island's volcanic

edifice (López et al., 2012) (Fig. 1). On 10 October at 04:10 UTC, a clear emergent tremor signal was registered by all the seismic stations indicating the onset of the eruptive activity that lasted for more than four months (until the end of February 2012) (López et al., 2014).

4. Datasets

4.1 Spatial analysis

A susceptibility analysis enables us to determine the probability of occurrence of future eruptive vents. This probability depends on the volcano-structural elements that define the structural setting of a volcano and the past pathways taken by the magma as it ascended to the Earth's surface. Eruptive vents and fissures, dykes, faults, fumaroles, and the stress field are the most important elements (Martin et al., 2004; Jaquet et al., 2008; Cappello et al., 2012; Bartolini et al., 2013; and references therein) that determine the probabilities of an eruptive vent opening in an area that was affected by similar types of eruptions in the past.

In order to compute the probability of opening a new eruptive vent at El Hierro, we took into account the most relevant volcano-structural data as given by Becerril et al. (2013, 2014) (Fig. 2): (i) the subaerial vents and eruptive fissures that are part of the Rift Volcanism (including sub-recent and recent eruptions) and (ii) the submarine vents and eruptive fissures deduced from bathymetric inference. Furthermore, we chose only those eruptive fissures oriented between N00ºE and N45ºE in relation to the orientation of the regional stress field (see Geyer et al., 2016). We assumed that the stress field plays the most important role in determining where the magma will reach the surface and the fractures orientated in this direction were those that offered the least resistance to magma transport.

200 To conduct the short-term analysis, we complemented the previous dataset with
201 the addition of data on the evolution of the seismicity for the unrest period (19 July
202 2011–10 October 2011).
203 We assumed that in this short-term spatial analysis the location of the seismicity
204 reflected the position of the magma, as it provides a good indicator for tracking magma
205 migration and for determining where it may potentially reach the surface. However, the
206 location of gas emission was not considered in this short-term analysis as they were too
207 disperse in the whole area (López et al., 2012) and thus not sufficiently informative on
208 the position that magma could have below the island. Concerning the surface
209 deformation, we considered this parameter only in the temporal analysis, due to the lack
210 of a well-distributed ground deformation monitoring network operating during the El
211 Hierro unrest episode. So, as described in López et al. (2012), the highest values of
212 uplift were found in the area where the seismicity moved from north to south and where
213 no GPS was available.
214 Seismic data was obtained from the seismic catalogue published by the Spanish
215 National Geographical Institute (IGN) (www.ign.es) (Fig. 2). Data were grouped in time
216 windows of four days to optimize the forecast given that certain volcanic systems have
217 indicated that magmatic processes have a memory with a time-scale of just a few days.
218 (Connor et al., 2003; Jaquet and Carniel, 2003; Jaquet et al., 2006; Tárraga et al., 2006;
219 Carniel et al., 2006). Such a selection allows assuring the persistent behaviors of the
220 system. Within the time window, the seismic activity will follow the same trend of
221 previous days, allowing the short-term forecast. We selected from the IGN catalogue
222 only those earthquakes of magnitudes greater than zero and precise locations, with
223 epicenter maximum semi-ellipse axes of less than 15 km, minimum semi-ellipse axes of
224 less than 6 km, and a depth error of less than 8 km. In this way, we aimed to avoid –

225 inasmuch as was possible – errors in the hypocenter localization of earthquakes due to
226 the small number of the seismic stations in place during the first unrest phase.
227
228 4.2 Temporal analysis
229 The data for the temporal analysis consisted of observables which relative variation
230 with time may indicate changes in the processes occurring inside the volcano when
231 preparing for a new eruption (Sobradelo and Martí, 2015; Bartolini et al., 2016). In our
232 methodology, we do not use the absolute values of each parameter, but considering their
233 relative variation with time, we only indicate if there is an increase or a decrease in the
234 value of such parameter in each time interval. We used the monitoring data gathered by
235 the IGN and other published information (López et al., 2012, 2014; Martí et al., 2013;
236 Telesca et al., 2014). This information is given in Table 1 and includes:
237 - the number of seismic events
238 - RSAM (Real-time Seismic Amplitude Measurement)
239 - the seismic energy released during the fracturing process
240 - the lateral and vertical migration of the seismicity
241 - the number of shallow seismic events
242 - the strain variation.
243 Therefore, consistent with the choices adopted for the spatial analysis, the
244 variation in the unrest indicators (increase/decrease) was evaluated in relation to the
245 mean values for the previous four days. The seismic rate variation was considered by
246 taking into account only those events with a magnitude over 2.5 (greater than the
247 completeness magnitude during almost all the period), assuring this way the study of the
248 seismic evolution (López et al., 2017), while a significant change was considered only
249 when the rate of variation was 25% higher in relation to the previous four days as a

consequence of stress reorganization (Stein, 1999). RSAM data was obtained by analyzing the signal registered by the vertical component of the seismic broadband CTIG station (Fig. 1). Although the signal may have a high background of seismic noise, a RSAM increase is a good indicator of the transport of the magma to the surface (Endo and Murray, 1991). In order to highlight a significant increase in RSAM values, we considered the variation in the slope of the inverse of the RSAM, which is clear evidence of a consistent increase in the signal. The accumulated increase in energy release was considered to be significant when the energy value (i.e. the accumulated value in relation to the mean value over the last four days) was greater than 10%. In this case, the accumulated energy curve showed a notable slope variation. For the lateral migration of the seismicity, we considered a significant variation to exist when the displacement increment was over 1 km. This is compatible with the effects on hazard scenarios when the vent location changes. The vertical migration of the seismicity ranges from a depth of approximately 19 km to the surface and, taking into account the mean of the variation, a variation greater than 0.6 km was assumed to be notable. The number of shallow events reflects the presence of the magma close to the surface and so we assumed that the number of events of magnitude greater than 3 in the same day at a depth of 0–5 km was significant. Finally, the strain variation has been determined with the horizontal components data of the GPS FRON station. We have assumed a significant variation when the increase/decrease was greater than 1.5 mm of the vector representing the horizontal deformation (composing the north and east GPS components).

5. Results

5.1 Spatial probability of new vent opening

Given its great flexibility and ability to identify the most likely zones to host new eruptions in monogenetic volcanic fields, we used the QVAST tool (Bartolini et al., 2013) to determine the susceptibility from the evolution of the seismicity during the unrest. This tool was applied first to evaluate the smoothing factors or bandwidths of the dataset analysed, then to evaluate the probability density functions for each dataset, and, finally, to calculate the final susceptibility map (Fig. 3) (see also Figure S1). The bandwidth is a free smoothing parameter included in the kernel function that we used to estimate the corresponding probability density functions and determines how probabilities are distributed in terms of the distance from the volcanic structures or vents (Martí and Felpeto, 2010; Bartolini et al., 2013).

In the case of the rift volcanism and the submarine layers, we applied the Least Square Cross Validation Method (LSCV) (Cappello et al., 2012; Bartolini et al., 2013) to obtain the bandwidth parameter, as it better represents the geometry of the vents distribution, NE-SW elongated (see Becerril et al. (2013)). To determine the influence of seismicity in the spatial analysis, we considered that the most representative result was that obtained using Silverman's Rule of Thumb for the optimal bandwidth (Silverman, 1986). In fact, the result obtained using this method allows describing the spatial seismicity swarm distribution for the entire period, avoiding to underestimate the influence area (located close to the epicentral points) and to overestimate the density estimation (high values of the density distribution caused by small bandwidth values). Thus, we obtained a bandwidth value of 1100 m for the rift volcanism and of 3900 m for the submarine layer, while in the case of the seismic data the range in the degree of randomness was from 500 m to 1500 m.

In the evaluation of the final susceptibility, weights were assigned based on expert opinion and on previously published work (Becerril et al., 2013, 2014), and by taking into account the average depth of the seismicity during the unrest episode. In detail, the relevance and reliability values (Table 3) (Martí and Felpeto, 2010) have been assigned as follow: relevance was given through an elicitation of expert judgment procedure (Aspinall, 2006) among the members of the Group of Volcanology of Barcelona (GVB-CSIC) and external collaborators; reliability was considered as maximum in all the datasets (value of 1).

Specifically, up to 7 October we observed no significant variation in the shallow seismicity (Table 1). In this case, we assigned the following weights: 0.5 for seismic events, 0.3 for onshore vents and fissures, and 0.2 for offshore vents and fissures. In the final period (8–10 October), we considered the shallow earthquakes as a separate layer by assigning a different and more consistent weight as follows: 0.6 for shallow seismic events, 0.2 for the remaining seismic events, 0.1 for onshore vents and fissures, and 0.1 for offshore vents and fissures.

The results shown in Figure 3 (see also Figure S1) highlight the importance of combining monitoring data with a previous long-term hazard assessment as a means of updating the probability of a new eruptive vent appearing in a particular area. The presence of previous volcanic structures does not provide sufficient information for forecasting the possible opening of a fresh vent during the unrest phase; however, if this information is combined with ongoing seismicity the predicted result can be improved. As shown in Figure 3, before the eruption the area with the highest probability of a fresh vent opening is the area that is closest to the eruptive vent.

5.2 Evolution of unrest indicators and short-term hazard assessment

The temporal analysis of the unrest indicators was conducted by applying the ST-HASSET tool (Bartolini et al., 2016) to analyze possible patterns in the evolution of events preceding the submarine eruption on El Hierro. The advantages of this tool lie in its ability to consider different signals on the same probabilistic scale, based on any significant or abnormal change in the unrest signal, with respect to a previous stage and/or a base-line measurement considered normal. The tool computes at each stage the probability of experiencing an anomalous change (increase/decrease) by the next time bulletin, based on what has been observed up until now. With this, it helps the scientist sum up the evolution of the unrest indicators and gets some insight into the possible unfolding of the volcanic crisis in the immediate future, helping with decision-making and the interpretation of the unrest. In Table 1, we show the data for the entire unrest period and, as explained in section 3.2.2, we considered the variation ("Y") of the indicator analysed based on different criteria. The choice of the aleatoric and epistemic uncertainties (prior and data weigths) surrounding the probability estimates were assumed considering that El Hierro unrest was the first unrest registered in Canaries. The prior weights were assumed to be the probability results of the previous bulletin (only in the first simulation we have assumed the same probability for each indicator). In the case of the data weights, we have first assigned a total epistemic uncertainty and sequentially incremented the weight with the evolution of the unrest.

In Figure 4 and Movie S1, the evolution of the indicators over the entire unrest period with a daily time window are clearly visible. In the right side of the chart, it is shown also day-by-day the total number of parameters that increase or descrease during the unrest evolution. We assumed a value of +1 if the indicator increases, -1 if the indicator decreases, and 0 if the change is not significant. This allows visualizing the overall tendency of variation of the unrest indicators. We also considered three phases

of 28 days, all three during the evolution of the unrest period, as shown in Figure 5 and so were able to observe how these indicators varied in different ways as the unrest evolved:

- Phase I: from July 19th to August 15th;
- Phase II: from the August 16th to September 12th;
- Phase III: from September 13th to October 10th.

By having all the precursory activity mapped and plotted into the same graph, it is easier to interpret their evolution as a whole. According to what was been defined as a significant change, in a first phase the accumulated energy released increase (AERI) and the lateral migration of seismicity (LMS) experienced a significant change, and continued overall the increasing tendency across this initial phase with periods of no significant variation followed by periods of heavy changes. By the time, they enter the second phase both indicators show no changes seem stable until well into the third phase where AERI starts experiencing significant increases and LMS follows a few days later. As per the other indicators, in a first phase they all experience a significant change at some point in the initial stages of Phase I and seem to enter a quiet phase after that, except for the RSAM, which on average experiences a continuous increase across the three phases, perhaps more consistent though Phases II and III. The unrest indicators that seem to experience larger significant changes in Phase I are AERI, LMS and RSAM.

Phase II was characterized by an overall stabilization of the indicators, except for RSAM that continues to consistently increase. In addition, by the middle of this second phase the seismicity experiences a significant increase with a small period of significant lateral migration of seismicity, followed by a small jump in the RSAM a few days later. By the time the systems enters into the phase III on September 12 we

continue to observe a probability increase in RSAM with a new significant jump around the September 18. This change happens simultaneously with a significant LMS increase for the first time since phase I, and a jump in the seismicity increase followed by an AERI jump and strain variation. There seems to be a clear inflection point around the 20th of September. This point is the first time since the beginning of the unrest three months ago where all unrest indicators show consistently significant changes at once. This suggests that the system has changed and is getting ready to enter into a new eruptive phase. Note that a few days before the submarine eruption there is a jump in all the indicators including for the first time the shallow seismicity and the vertical migration of seismicity, the probabilities for these two continue to increase from this moment onwards, together with RSAM, while LMS and AERI remain constant.

6. Discussion and Conclusions

Short-term hazard assessment should be always conducted based on a previous long-term hazard assessment, as a systematic study of past eruptive activity conducted well before a new volcanic crisis starts can help forecast the most probable scenarios and thus avoid confusion regarding the potential outcome of the forthcoming eruption.

In the case of El Hierro, unfortunately, no previous hazard assessment existed, so the most probable scenario – a submarine eruption – was not anticipated, as has been shown by a subsequent study (Becerril et al., 2014). Consequently, scientific advisors and decision-makers considered possible eruptive scenarios that had much lower probabilities of occurrence, which implied the taking of decisions with a higher cost than necessary (Sobradelo et al., 2014).

Via a retrospective analysis of the particular case of El Hierro, the results obtained in this work provide an easy and useful approach to the understanding and

visualization of the information recorded by the monitoring system, and show how this information can be used to forecast an eruption and its potential hazards in real time. The translation of this information into a coherent picture that will be helpful for anticipating the future evolution of a volcanic system is not straightforward, which is why we propose that this simple methodology be used to facilitate communication among scientists and between scientists and decision-makers. Moreover, the interpretation of unrest indicators and the observation of significant variations in volcanic systems are complex tasks subject to great uncertainties and the approach proposed in this work aims to act as a guide for experts and decision-makers to be employed as a crisis unfolds.

Another important aspect is how to interpret monitoring signals in monogenetic volcanism. In this specific case, where the location of a future eruption is not easy to determine, the spatial probability is controlled by local and regional stress fields that are usually poorly understood. During the pre-eruptive episode on El Hierro, it was clear that the lateral migration of the magma was controlled by the presence of stress barriers defined by major structural and rheological discontinuities (Martí et al. 2013, 2017). This gave rise to nearly continuous changes in the probable location of the eruptive vent, which hindered the definition of a precise eruptive scenario and the application of appropriate mitigation measures. This highlights the importance of understanding monitoring signals and their interactions, as well as the need for knowledge of the past activity of the volcanic system in the form of susceptibility and hazard analyses, if a volcanic eruption is to be correctly forecast. In case of El Hierro, the susceptibility map that combines volcano-structural information and seismic data (Fig. 3) shows how the possible location of a eruptive vent varied during the evolution of the pre-eruptive unrest: initially, the magma was thought to be accumulating on the northern side of the

424 island (Fig. 3b) but in the end it was concentrated on the southern side (Fig. 3d), where
425 it eventually provoked a submarine eruption. This confirms the idea that seismic activity
426 and ground deformation are good indicators of magma location in monogenetic
427 volcanism.

428 The analysis of the precursors shows how special attention should be paid to
429 each one during the evolution of the unrest period (Fig. 4). Indeed, in the initial phase,
430 we observed obvious fluctuations in most indicators and, above all, an increase in the
431 accumulated energy released compared to the background level. In the second phase,
432 the behavior of these indicators remained constant and there was no significant spread, a
433 reflection of how the magma followed the local stress field and migrated from the north
434 to the southeast. During the final month before the eruption, we noted that the indicators
435 started to increase sequentially but at the same hypocentral depth. However, in the final
436 hours before the eruption the presence of very shallow seismicity indicated that,
437 immediately after the final major earthquake, a relatively rapid vertical migration of
438 magma was taking place. This vertical ascent to the surface was associated with a
439 drastic decrease in both the number of seismic events (almost no seismicity of any kind
440 in the 30 hours before the onset of the eruption) in the accumulated energy release, and
441 in the deformation, but also with an increase in the RSAM, thereby suggesting that the
442 final major tectonic earthquake facilitated a path for the magma to reach the surface
443 (Martí et al., 2013).

444 From an emergency management perspective, it is worth stressing two further
445 important results of the application of our method. Firstly, it identified unmistakably the
446 anomalous behavior of the activity, characterized by an increasing probability in almost
447 all indicators during the first days of the unrest period as they varied in relation to the
448 background values. Secondly, many indications suggested that the probability of an

449 eruption increased in almost all parameters from 25 September until the onset of the
450 eruption. On 23–27 September, the Canarian Civil Protection Authorities in charge of
451 the management of the volcanic crisis changed the alert level for the population from
452 Green to Yellow in two areas due to the strong seismicity being felt by the population
453 and the risk of rock falls near populated areas. In 10 October, the appearance of an
454 increasingly strong seismic tremor signal in the monitoring network warned of the
455 imminent onset of the eruption and Civil Protection raised the alert level to Red.
456 Despite the correct management of the eruption crisis on El Hierro by the Canarian
457 Civil Protection, we still believe that our results can improve significantly the island's
458 early warning capability during an unrest period characterized by a high level of
459 uncertainty. Thus, the tools presented here could have been very useful for the Canarian
460 Civil Protection during the October 2011 eruption crisis.
461
462 **Acknowledgements:** This research was funded by the European Commission (EC
463 ECHO Grant SI2.695524: VeTOOLS). The authors would like to thank the Instituto
464 Geográfico Nacional (IGN - Madrid) and, especially, Rafael Abella Meléndez, for the
465 ease in accessing the monitoring data. Joan Martí is grateful for the MECD
466 (PRX16/00056) grant. The English text was edited by Michael Lockwood.
467
468
469
470
471
472
473

References

Bartolini, S., Cappello, A., Martí, J., and Del Negro, C.: QVAST: a new Quantum GIS plugin for estimating volcanic susceptibility, Nat. Hazards Earth Syst. Sci., 13, 3031–3042, doi:10.5194/nhess-13-3031-2013, 2013.

Bartolini, S., Sobradelo, R., and Martí, J.: ST-HASSET for volcanic hazard assessment: A Python tool for evaluating the evolution of unrest indicators, Computers & Geosciences, doi:10.1016/j.cageo.2016.05.002, 2016.

Becerril, L., Cappello, A., Galindo, I., Neri, M., and Del Negro, C.: Spatial probability distribution of future volcanic eruptions at El Hierro Island (Canary Islands, Spain), J. Volcanol. Geoth. Res., 257, 21–30, doi:10.1016/j.jvolgeores.2013.03.005, 2013.

Becerril, L., Bartolini, S., Sobradelo, R., Martí, J., Morales, J.M., and Galindo, I.: Long-term volcanic hazard assessment on El Hierro (Canary Islands), Natural Hazards and Earth System Science, 14, 1853-1870, 2014.

Blong, R.: Volcanic hazards and risk management, in Encyclopedia of volcanoes, edited by H. Sigurdsson et al., pp. 1215–1227, Academic, San Diego, 2000.

Bosshard, E., and MacFarlane, D.J.: Crustal structure of the western Canary Island from seismic refraction and gravity data, J. Geophys. Res., 75, 4901-4918, 1970.

Cappello, A., Neri, M., Acocella, V., Gallo, G., Vicari, A., and Del Negro, C.: Spatial vent opening probability map of Etna volcano (Sicily, Italy), Bull. Volcanol., 74, 2083–2094, doi:10.1007/s00445-012-0647-4, 2012.

Carniel, R., Tárraga, M., Jaquet, O., and García, A.: On the memory of seismic noise recorded at Teide-Pico Viejo volcanic complex, Tenerife, Spain, EGU06-A-01929; NH5.03-1WE2P-0679, EGU General Assembly, Vienna, 2006.

Chouet, B.: Long period volcano seismicity: Its source and use in eruption forecasting, Nature, 380, 309-316. doi: 10.1038/380309a0, 1996.

Connor, C.B., and Conway, F.M.: Basaltic Volcanic Fields, in Encyclopedia of Volcanology. Academic Press, pp. 331-343, 2000.

Connor, C.B., Sparks, R.S.J., Mason, R.M., Bonadonna, C., and Young, S.R.: Exploring links between physical and probabilistic models of volcanic eruptions: The Soufrière Hills Volcano, Montserrat, Geophys. Res. Lett., 30, 1701. doi:10.1029/2003GL017384, 13, 2003.

Domínguez Cerdeña, I., del Fresno, C., and Gomis Moreno, A.: Seismicity patterns prior to the 2011 El Hierro eruption, Bull. Seismol. Soc. Am. 104, 567–575, doi:10.1785/0120130200, 2014.

Endo, T. E., and Murray, T.: Real-time Seismic Amplitude Measurement (RSAM). A volcano monitoring and prediction tool, Bull. Volcanol., 53, 533–545, 1991.

Geyer, A., Martí, J., and Villaseñor, A.: First-order estimate of the Canary Islands plate-scale stress field: Implications for volcanic hazard assessment, Tectonophysics, doi:10.1016/j.tecto.2016.04.010, 2016.

Guillou, H., Carracedo, J.C., Pérez-Torrado, F.J., and Rodríguez Badiola, E.: K-Ar ages and magnetic stratigraphy of a hotspot- induced, fast grown oceanic island: El Hierro, Canary Islands, J. Volcanol. Geoth. Res. 73, 141–155, 1996.

Harrington, R.M., and Brodsky, E.E.: Volcanic hybrid earthquakes that are brittle-failure events, Geophys. Res. Lett., 34, L06308, doi:10.1029/2006GL028714, 2007.

Jaquet, O., and Carniel, R.: Multivariate stochastic modelling: towards forecasts of paroxysmal phases at Stromboli, J. Volcanol. Geotherm. Res., 128(1–3), 261–271, 2003.

Jaquet, O., Sparks, R.S.J., and Carniel, R.: Magma memory recorded by statistics of volcanic explosions at the Soufrière Hills Volcano, Montserrat in Statistics in

Volcanology, Special Publications of IAVCEI, edited by Mader, H.M., S. Coles, and C. Connor, vol. 1, pp. 175–184, 2006.

Jaquet, O., Connor, C.B., and Connor, L.: Probabilistic Methodology for Long Term Assessment of Volcanic Hazards, IHLRMW, Las Vegas, USA, 2008.

Jellineck, A.M., and Bercovici, D.: Seismic tremors and magma wagging during explosive volcanism, Nature, 470, 522–526, 2011.

Kereszturi, G. and Németh, K.: Monogenetic Basaltic Volcanoes: Genetic Classification, Growth, Geomorphology and Degradation, in Updates in Volcanology-New Advances in Understanding Volcanic Systems, edited by K. Németh, pp. 3-88, InTech, doi:10.5772/51387, 2012.

Klügel, A., Hansteen, T.H., and Galipp, K.: Magma storage and underplating beneath Cumbre Vieja volcano, La Palma (Canary Islands), Earth and Planetary Science Letters 236, 211–226, 2005.

Lavallée, Y., Meredith, P.G., Dingwell, D.B., Hess, K.U., Wassermann, J., Cordonnier, B., Gerik, A., and Kruhl, J.H.: Seismogenic lavas and explosive eruption forecasting, Nature, 453, 507–510, 2008.

López, C., Blanco, M.J., Abella, R., Brenes, B., Cabrera-Rodríguez, V.M., Casas, B., Domínguez-Cerdeña, I., Felpeto, A., Fernández de Villalta, M., del Fresno, C., García, O., García-Arias, M.J., García-Cañada, L., Gomis-Moreno, A., González-Alonso, E., Guzmán-Pérez, J., Iribarren, I., López-Díaz, R., Luengo-Oroz, N., Meletlidis, S., Moreno, M., Moure, D., Pereda de Pablo, J., Rodero, C., Romero, E., Sainz-Maza, S., Sentre-Domingo, M.A., Torres, P.A., Trigo, P., and Villasante-Marcos, M.: Monitoring the unrest of El Hierro (Canary Islands) before the onset of the 2011 Submarine Eruption, Geophys. Res. Lett., 39, L13303, doi:10.1029/2012GL051846, 2012.

López, C., Martí, J., Abella, R., and Tárraga, M.: Applying fractal dimensions and energy-budget analysis to characterize fracturing processes during magma migration

574 and eruption: 2011–2012 El Hierro (Canary Islands) submarine eruption, Surv.
575 Geophys. 1–22, doi:10.1007/s10712-014-9290-2, 2014.
576
577 López, C., Benito-Saz, M. A., Martí, J., del-Fresno, C., García-Cañada, L., Albert, H.,
578 Lamolda, H.: Driving Magma to the Surface: the 2011–2012 El Hierro Volcanic
579 Eruption. Geochemistry, Geophysics, Geosystems (submitted).
580 Martí, J., Pinel, V., López, C., Geyer, A., Abella, R., Tárraga, M., Blanco, M.J., Castro,
581 A., and Rodríguez, C.: Causes and mechanisms of the 2011–2012 El Hierro (Canary
582 Islands) submarine eruption, J. Geophys. Res. B: Solid Earth, 118(3), 823–839.
583 doi:http://dx.doi.org/10.1002/jgrb.50087, 2013.
584
585 Martí, J., López, C., Bartolini, S., Becerril, L., and Geyer, A.: Stress controls of
586 monogenetic volcanism: a review, Frontiers in Earth Sciences, 4(106). doi:
587 10.3389/feart.2016.0010, 2016.
588
589 Martí, J., A. Villaseñor, A. Geyer, C. López, and Tryggvason, A.: Stress barriers
590 controlling lateral migration of magma revealed by seismic tomography, Scientific
591 Reports, 7, 40757, doi: 10.1038/srep40757, 2017.
592
593 Martin, A.J., Umeda, K., Connor, C.B., Weller, J.N., Zhao, D., and Takahashi, M.:
594 Modeling long-term volcanic hazards through Bayesian inference: an example from the
595 Tohuku volcanic arc Japan, J. Geophys. Res., 109, B10208,
596 doi:10.1029/2004JB003201, 2004.
597
598 Marzocchi, W., Sandri, L., and Selva, J.: BET_EF: A probabilistic tool for long- and
599 short-term eruption forecasting, Bull. Volcanol., 70, 623–632, 2008.
600
601 McNutt, S.: Seismic monitoring and eruption forecasting of volcanoes: A review of the
602 state of the art and case histories, in Monitoring and mitigation of volcano hazards,
603 edited by Scarpa and Tilling, Springer, Berlin, 99–146, 1996.
604
605 McNutt, S. R.: Volcano Seismology, Ann. Rev. Earth Planet. Sci., 33, 461-491, 2005.
606

607 Neuberg, J., Luckett, R., Baptie, B., and Olsen, K.: Models of tremor and low-frequency
608 earthquake swarms on Montserrat, J. Volcanol. Geoth. Res., 101, 83–104, 2000.
609
610 Papale, P.: Strain-induced magma fragmentation in explosive eruptions, Nature 397,
611 425–428, 1999.
612
613 Phillipson, G., Sobradelo, R., and Gottsmann, J.: Global volcanic unrest in the 21st
614 century: An analysis of the first decade, J. Volcanol. Geoth. Res., 264, 183–196, 2013.
615
616 Ranero, C.R., Torne, M., and Banda, E.: Gravity and multichannel seismic reflection
617 constraints on the lithospheric structure of the Canary swell, Mar. Geophys. Res., 17,
618 519-534, 1995.
619
620 Scarpa, R., and Tilling, R.I.: Monitoring and Mitigation of Volcano Hazards: Berlin,
621 Springer-Verlag, 1996.
622
623 Silverman, B.W.: Density Estimation for Statistics and Data Analysis, Chapman & Hall,
624 London, 1986.
625
626 Sparks, R.S.J.: Forecasting volcanic eruptions, Earth Planet. Sci. Lett., 210, 1–15, 2003.
627
628 Sobradelo, R., Martí, J., Kilburn, C., and López, C.: Probabilistic approach to decision-
629 making under uncertainty during volcanic crises: retrospective application to the El
630 Hierro (Spain) 2011 volcanic crisis, Nat. Hazards, doi:10.1007/s11069-014-1530-8,
631 2014.
632
633 Sobradelo, R., and Martí, J.: Short-term volcanic hazard assessment through Bayesian
634 inference: Retrospective application to the Pinatubo 1991 volcanic crisis, Journal of
635 Volcanology and Geothermal Research, 290, 1–11, 2015.
636
637 Stein, R.: The role of stress transfer in earthquake occurrence, Nature 402, 605–609,
638 1999.
639

Stroncik, N. A, Klügel, A., and Hansteen, T.H.: The magmatic plumbing system beneath El Hierro (Canary Islands): constraints from phenocrysts and naturally quenched basaltic glasses in submarine rocks. Contrib. Mineral. Petrol., 157, 593-607, doi:10.1007/s00410-008-0354-5, 2009.

Tárraga, M., Carniel, R., Ortiz, R., Marrero, J.M., and García, A.: On the predictability of volcano- tectonic events by low frequency seismic noise analysis at Teide-Pico Viejo volcanic complex, Canary Islands, Natural Hazards and Earth System Science, 6(3), 365-376, 2006.

Tárraga, M., Martí, J., Abella, R., Carniel, R., and López, C.: Volcanic tremors: good indicators of change in plumbing systems during volcanic eruptions, J. Volcanol. Geotherm. Res., 273, doi:j.jvolgeores.01.003, 2014.

Telesca, L., Lovallo, M., Martí, J., López, C., and Abella, R.: Using the Fisher–Shannon method to characterize continuous seismic signal during volcanic eruptions: application to 2011–2012 El Hierro (Canary Islands) eruption. Revealing dynamic changes on El Hierro (Canary Islands) during the 2011–2012 eruption through investigation of the continuous seismic signal. Terra Nova, 26, 425–429, 2014.

Telesca, L., Lovallo, M., Martì, J., López, C., and Abella, R.: Multifractal investigation of continuous seismic signal recorded at El Hierro volcano (Canary Islands) during the 2011–2012 pre- and eruptive phases, Tectonophysics, 642, 71–77, 2015.

Tonini, R., Sandri, L., Rouwet, D., Caudron, C., Marzocchi, W., and Suparjan: A new Bayesian Event Tree tool to track and quantify volcanic unrest and its application to Kawah Ijen volcano, Geochem. Geophys. Geosyst., 17, 2539–2555, doi:10.1002/2016GC006327, 2016.

Valentine, G.A., and Gregg, T.K.P.: Continental basaltic volcanoes-processes and problems, J. Volcanol. Geotherm. Res., 177(4), 857–873, 2008.

672 Vallianatos, F., Michas, G., Papadakis, G., and Tzanis, A.: Evidence of non-extensivity
673 in the seismicity observed during the 2011–2012 unrest at the Santorini volcanic
674 complex, Greece, Nat. Hazards Earth Syst. Sci., 13, 177–185, 2013.
675
676 Watts, A.B.: Crustal structure, gravity-anomalies and flexure of the lithosphere in the
677 vicinity of the Canary-Islands. Geophys. J. Int. 119 (2), 648-666, doi:10.1111/j.1365-
678 246X.1994.tb00147.x, 1994.
679
680
681
682
683
684
685
686
687
688
689
690
691
692
693
694
695
696
697
698

699 **Table**

700 Table 1. Unrest indicators during the unrest period.

701

702 **Figures**

703 Figure 1. IGN monitoring network during the unrest period at El Hierro Island. The top
704 left inset displays the location of El Hierro within the Canary Archipelago.

705 Figure 2. Structural data of El Hierro (vents and fissure onshore and offshore, as in
706 Becerril et al. 2013, 2014) and the evolution of the seismicity during the unrest period
707 (average location of the seismic swarm).

708 Figure 3. Susceptibility maps obtained from: a) the volcano-structural data; b) the first
709 days of unrest; c) in the middle of the unrest; d) the days before the submarine eruption.

710 Figure 4. ST-HASSET: the evolution of the unrest indicators in three phases of 28 days.
711 The right side of the chart shows day-by-day the tendency of variation of the unrest
712 indicators.

713 Figure 5. ST HASSET: the evolution of all indicators every 28 days (3 phases of
714 unrest).

715

716 **Supplementary Material**

717 Figure S1 - Susceptibility maps and seismicity location during the evolution of the
718 unrest period.

719 Movie S1 - Evolution of the unrest indicators and its registered values.

Table 1

UNREST INDICATORS	SEISMICITY INCREASE			RSAM ACCELERATION INCREASE			ACCUMULATED ENERGY RELEASED INCREASE			LATERAL MIGRATION OF SEISMICITY			VERTICAL MIGRATION OF SEISMICITY			SHALLOW SEISMICITY			STRAIN VARIATION		
	Y/N/na	Value [n°]	Probability	Y/N/na	Value [1/RSAM unit]	Probability	Y/N/na	Value [J]	Probability	Y/N/na	(Figure 2)	Probability	Y/N/na	Value [km]	Probability	Y/N/na	Value [n°]	Probability	Y/N/na	Value [m]	Probability
2011-07-19	N	0	0.333	N	0.041	0.333	N	5.80E+07	0.333	N		0.333	N	12	0.333	N	0	0.333	N	0.012	0.333
2011-07-20	N	0	0.25	N	0.042	0.250	Y	2.41E+08	0.500	Y		0.500	N	11.88	0.250	N	0	0.25	N	0.014	0.25
2011-07-21	N	0	0.2	N	0.039	0.200	Y	1.72E+09	0.600	N		0.400	N	10.78	0.200	N	0	0.2	N	0.015	0.2
2011-07-22	N	0	0.167	N	0.043	0.167	Y	3.18E+09	0.667	N		0.333	N	10.09	0.167	N	0	0.167	N	0.015	0.167
2011-07-23	N	0	0.143	N	0.047	0.143	Y	2.15E+09	0.715	Y		0.428	N	10.72	0.143	N	0	0.143	N	0.014	0.143
2011-07-24	N	0	0.125	N	0.051	0.125	Y	4.30E+08	0.751	Y		0.499	N	10.53	0.125	N	0	0.125	N	0.012	0.125
2011-07-25	N	0	0.111	N	0.054	0.111	Y	5.73E+08	0.779	Y		0.555	Y	13.4	0.222	N	0	0.111	N	0.014	0.111
2011-07-26	N	0	0.1	N	0.053	0.100	Y	1.50E+09	0.801	N		0.499	N	8.45	0.200	N	1	0.1	N	0.014	0.1
2011-07-27	Y	2	0.182	N	0.052	0.091	Y	3.00E+09	0.819	N		0.454	N	8.93	0.182	Y	4	0.182	N	0.015	0.091
2011-07-28	N	0	0.167	Y	0.055	0.167	Y	7.27E+08	0.834	N		0.416	N	10.33	0.167	N	1	0.167	N	0.016	0.083
2011-07-29	N	0	0.154	Y	0.044	0.231	N	1.79E+08	0.770	N		0.384	N	12.75	0.154	N	0	0.154	N	0.016	0.077
2011-07-30	N	0	0.143	Y	0.036	0.286	N	6.17E+08	0.715	N		0.357	Y	11.82	0.214	N	0	0.143	N	0.018	0.071
2011-07-31	N	0	0.133	N	0.035	0.267	N	1.22E+09	0.667	N		0.333	N	11.18	0.200	N	0	0.133	na	na	0.071
2011-08-01	N	0	0.125	N	0.039	0.250	N	1.75E+08	0.625	N		0.312	N	12	0.188	N	0	0.125	N	0.020	0.067
2011-08-02	N	0	0.118	N	0.047	0.235	N	4.60E+08	0.588	Y		0.352	N	10.67	0.177	N	0	0.118	N	0.017	0.063
2011-08-03	N	0	0.111	N	0.045	0.222	N	4.48E+08	0.555	Y		0.388	N	11.47	0.167	N	0	0.111	N	0.020	0.059
2011-08-04	N	0	0.105	N	0.042	0.210	Y	2.60E+09	0.578	Y		0.420	N	10.54	0.158	N	0	0.105	N	0.021	0.056
2011-08-05	N	0	0.1	N	0.038	0.199	Y	4.24E+09	0.599	Y		0.449	N	10.54	0.150	N	1	0.1	N	0.020	0.053
2011-08-06	N	0	0.095	N	0.041	0.190	Y	2.31E+08	0.618	Y		0.475	N	9.61	0.143	N	0	0.095	N	0.022	0.05
2011-08-07	N	0	0.091	N	0.056	0.181	Y	1.62E+09	0.635	N		0.453	N	10.45	0.136	N	3	0.091	Y	0.027	0.093
2011-08-08	N	0	0.087	Y	0.066	0.217	N	1.46E+09	0.607	N		0.433	N	11.16	0.130	N	1	0.087	N	0.022	0.089
2011-08-09	Y	1	0.125	Y	0.053	0.250	Y	4.38E+09	0.623	N		0.415	N	10.6	0.125	N	2	0.083	N	0.021	0.085
2011-08-10	N	0	0.12	Y	0.037	0.280	Y	1.58E+09	0.638	N		0.398	N	10.95	0.120	N	0	0.08	N	0.024	0.082
2011-08-11	N	0	0.115	N	0.035	0.269	N	4.12E+08	0.613	N		0.383	N	10.07	0.115	N	0	0.077	N	0.023	0.079
2011-08-12	N	0	0.111	N	0.037	0.259	N	2.72E+08	0.590	N		0.369	N	11.28	0.111	N	0	0.074	N	0.022	0.076
2011-08-13	N	0	0.107	N	0.036	0.250	N	6.22E+07	0.569	Y		0.392	N	10	0.107	N	0	0.071	N	0.021	0.073
2011-08-14	N	0	0.103	N	0.035	0.241	N	1.40E+09	0.549	Y		0.413	N	11.91	0.103	N	0	0.069	N	0.021	0.07
2011-08-15	N	0	0.1	N	0.038	0.233	N	6.61E+08	0.531	N		0.399	N	11.41	0.100	N	0	0.067	N	0.024	0.068
2011-08-16	N	0	0.097	N	0.041	0.225	N	1.73E+08	0.514	Y		0.418	N	11.47	0.097	N	0	0.065	N	0.023	0.066
2011-08-17	N	0	0.094	N	0.035	0.218	N	6.48E+07	0.498	Y		0.436	N	10.9	0.094	N	0	0.063	N	0.023	0.064
2011-08-18	N	0	0.091	N	0.044	0.211	N	4.55E+09	0.483	Y		0.453	N	10.39	0.091	N	2	0.061	N	0.023	0.062
2011-08-19	N	0	0.088	N	0.057	0.205	Y	2.16E+09	0.498	Y		0.469	N	10.32	0.088	N	2	0.059	N	0.023	0.06
2011-08-20	N	0	0.085	Y	0.065	0.228	N	1.75E+08	0.484	N		0.456	N	11.19	0.085	N	0	0.057	N	0.024	0.058
2011-08-21	N	0	0.083	Y	0.055	0.249	N	2.25E+09	0.471	N		0.443	N	11.12	0.083	N	0	0.055	N	0.025	0.056
2011-08-22	N	0	0.081	Y	0.044	0.269	N	2.72E+09	0.458	Y		0.458	N	11.12	0.081	Y	4	0.081	N	0.026	0.054
2011-08-23	N	0	0.079	Y	0.040	0.288	N	1.11E+09	0.446	Y		0.472	N	10.97	0.079	N	0	0.079	N	0.026	0.053
2011-08-24	N	0	0.077	N	0.041	0.281	N	3.55E+07	0.435	N		0.460	N	10.32	0.077	N	0	0.077	N	0.024	0.052
2011-08-25	N	0	0.075	N	0.051	0.274	N	2.55E+08	0.424	N		0.449	N	10.75	0.075	N	0	0.075	N	0.025	0.051
2011-08-26	N	0	0.073	N	0.058	0.267	N	5.73E+07	0.414	Y		0.462	N	10.9	0.073	N	0	0.073	N	0.026	0.05
2011-08-27	N	0	0.071	Y	0.062	0.284	N	1.17E+08	0.404	N		0.451	N	11.23	0.071	N	0	0.071	N	0.025	0.049
2011-08-28	N	0	0.069	Y	0.057	0.301	N	2.56E+07	0.395	N		0.441	N	10.95	0.069	N	0	0.069	N	0.028	0.048
2011-08-29	N	0	0.067	Y	0.041	0.317	N	2.42E+08	0.386	N		0.431	N	10.69	0.067	N	0	0.067	N	0.027	0.047
2011-08-30	N	0	0.066	N	0.049	0.310	N	8.00E+08	0.377	N		0.421	N	10.71	0.066	N	0	0.066	N	0.028	0.046
2011-08-31	N	0	0.065	N	0.084	0.303	N	7.45E+08	0.369	N		0.412	N	11.61	0.065	N	1	0.065	N	0.027	0.045
2011-09-01	Y	1	0.085	Y	0.122	0.318	N	4.35E+09	0.361	N		0.403	N	11.2	0.064	N	0	0.064	N	0.028	0.044
2011-09-02	Y	2	0.104	Y	0.090	0.332	N	3.96E+09	0.353	N		0.395	N	11.02	0.063	N	1	0.063	N	0.031	0.043
2011-09-03	N	0	0.102	Y	0.060	0.346	N	1.28E+09	0.346	N		0.387	N	11.14	0.062	N	1	0.062	N	0.030	0.042
2011-09-04	N	0	0.1	Y	0.054	0.359	N	8.43E+08	0.339	Y		0.399	N	10.79	0.061	N	0	0.061	N	0.030	0.041
2011-09-05	N	0	0.098	N	0.054	0.352	N	5.58E+08	0.332	Y		0.411	N	10.69	0.060	N	0	0.06	N	0.030	0.04
2011-09-06	N	0	0.096	N	0.049	0.345	N	7.45E+08	0.326	N		0.403	N	10.38	0.059	N	2	0.059	N	0.031	0.039
2011-09-07	N	0	0.094	N	0.055	0.338	N	1.40E+09	0.320	N		0.395	N	10.93	0.058	N	1	0.058	N	0.030	0.038
2011-09-08	N	0	0.092	Y	0.063	0.350	N	9.15E+08	0.314	N		0.388	N	10.94	0.057	N	1	0.057	N	0.030	0.037
2011-09-09	N	0	0.09	Y	0.056	0.362	N	1.60E+09	0.308	N		0.381	N	11.4	0.056	N	0	0.056	N	0.029	0.036
2011-09-10	Y	1	0.106	Y	0.047	0.373	N	1.88E+09	0.303	N		0.374	N	11.27	0.055	N	0	0.055	N	0.034	0.035
2011-09-11	N	0	0.104	N	0.051	0.366	N	6.27E+08	0.298	N		0.367	N	11.25	0.054	N	0	0.054	N	0.032	0.034
2011-09-12	Y	3	0.119	N	0.051	0.360	N	3.87E+09	0.293	N		0.361	N	11.19	0.053	N	0	0.053	N	0.034	0.033
2011-09-13	N	1	0.117	N	0.045	0.354	N	2.34E+09	0.288	N		0.355	N	11.55	0.052	N	0	0.052	N	0.033	0.032
2011-09-14	N	0	0.115	N	0.050	0.348	N	7.86E+08	0.283	N		0.349	N	11.4	0.051	N	0	0.051	N	0.038	0.031
2011-09-15	N	0	0.113	N	0.059	0.342	N	9.42E+08	0.278	Y		0.360	N	11.63	0.050	N	0	0.05	N	0.034	0.03
2011-09-16	N	0	0.111	Y	0.061	0.353	N	4.77E+08	0.274	N		0.354	N	12.07	0.049	N	0	0.049	N	0.036	0.03
2011-09-17	N	0	0.109	Y	0.050	0.363	N	5.50E+08	0.270	N		0.348	N	12.59	0.048	N	0	0.048	N	0.038	0.03
2011-09-18	N	0	0.107	Y	0.041	0.373	N	1.06E+09	0.266	N		0.343	N	12.76	0.047	N	0	0.047	N	0.038	0.03
2011-09-19	N	0	0.105	Y	0.039	0.383	N	5.71E+08	0.262	N		0.338	N	12.31	0.046	N	0	0.046	Y	0.042	0.045
2011-09-20	Y	8	0.119	Y	0.035	0.392	N	8.51E+09	0.258	N		0.333	N	12.57	0.045	N	0	0.045	N	0.041	0.044
2011-09-21	N	2	0.117	N	0.037	0.386	N	1.69E+09	0.254	N		0.328	N	12.53	0.044	N	1	0.044	N	0.041	0.043
2011-09-22	N	1	0.115	N	0.037	0.380	N	3.76E+09	0.250	N		0.323	N	12.98	0.043	N	0	0.043	Y	0.046	0.057
2011-09-23	Y	6	0.128	N	0.040	0.374	N	9.38E+09	0.246	N		0.318	N	13.37	0.042	N	1	0.042	N	0.046	0.056
2011-09-24	N	2	0.126	N	0.043	0.369	Y	1.19E+10	0.257	N		0.313	N	13.93	0.041	N	0	0.041	N	0.042	0.055
2011-09-25	N	2	0.124	N	0.065	0.364	Y	3.57E+09	0.267	N		0.309	N	12.82	0.040	N	0	0.04	N	0.047	0.054
2011-09-26	Y	11	0.136	Y	0.073	0.373	Y	1.21E+10	0.277	N		0.305	N	13.73	0.039	N	0	0.039	N	0.047	0.053
2011-09-27	Y	48	0.148	Y	0.041	0.382	Y	1.24E+11	0.287	Y		0.315	N	15.28	0.038	N	0	0.038	N	0.048	0.052
2011-09-28	Y	66	0.16	Y	0.039	0.390	Y	1.17E+11	0.297	Y		0.324	N	15.58	0.037	N	0	0.037	Y	0.048	0.065
2011-09-29	Y	49	0.171	Y	0.032	0.398	Y	1.57E+11	0.306	Y		0.333	Y	16.12	0.050	N	0	0.037	N	0.050	0.064
2011-09-30	N	21	0.169	N	0.053	0.393	Y	3.21E+10	0.315	Y		0.342	N	15.19	0.049	N	0	0.037	N	0.050	0.063
2011-10-01	N	27	0.167	N	0.064	0.388	Y	8.91E+10	0.324	Y		0.351	N	14.61	0.048	N	0	0.037	N	0.052	0.062
2011-10-02	Y	34	0.178	N	0.052	0.383	Y	6.85E+10	0.333	N		0.346	N	14.24	0.047	N	0	0.037	N	0.047	0.061
2011-10-03	Y	44	0.188	N	0.051	0.378	Y	9.37E+10	0.341	Y		0.354	N	14.58	0.046	N	0	0.037	Y	0.044	0.073
2011-10-04	N	17	0.186	Y	0.060	0.386	Y	4.76E+10	0.349	Y		0.362	N	14.82	0.045	N	0	0.037	N	0.048	0.072
2011-10-05	N	6	0.184	Y	0.051	0.394	N	2.63E+10	0.345	Y		0.370	N	14.97	0.044	N	0	0.037	N	0.053	0.071
2011-10-06	Y	34	0.194	Y	0.040	0.401	N	3.99E+10	0.341	Y		0.378	N	14.39	0.043	N	0	0.037	Y	0.055	0.082
2011-10-07	Y	27	0.204	Y	0.023	0.408	Y	1.18E+11	0.349	Y		0.385	N	13.56	0.042	N	0	0.037	Y	0.059	0.093
2011-10-08	N	12	0.202	Y	0.022	0.415	Y	2.11E+11	0.357	Y		0.392	Y	12.25	0.053	Y	7	0.048	Y	0.055	0.104
2011-10-09	N	3	0.2	Y	0.039	0.422	Y	1.95E+10	0.365	Y		0.399	Y	6.39	0.064	Y	34	0.059	N	0.054	0.103
2011-10-10	N	2	0.198	Y	0.004	0.429	N	2.00E+09	0.361	N		0.394	Y	11.55	0.075	Y	4	0.07	N	0.056	0.102

Figure 1

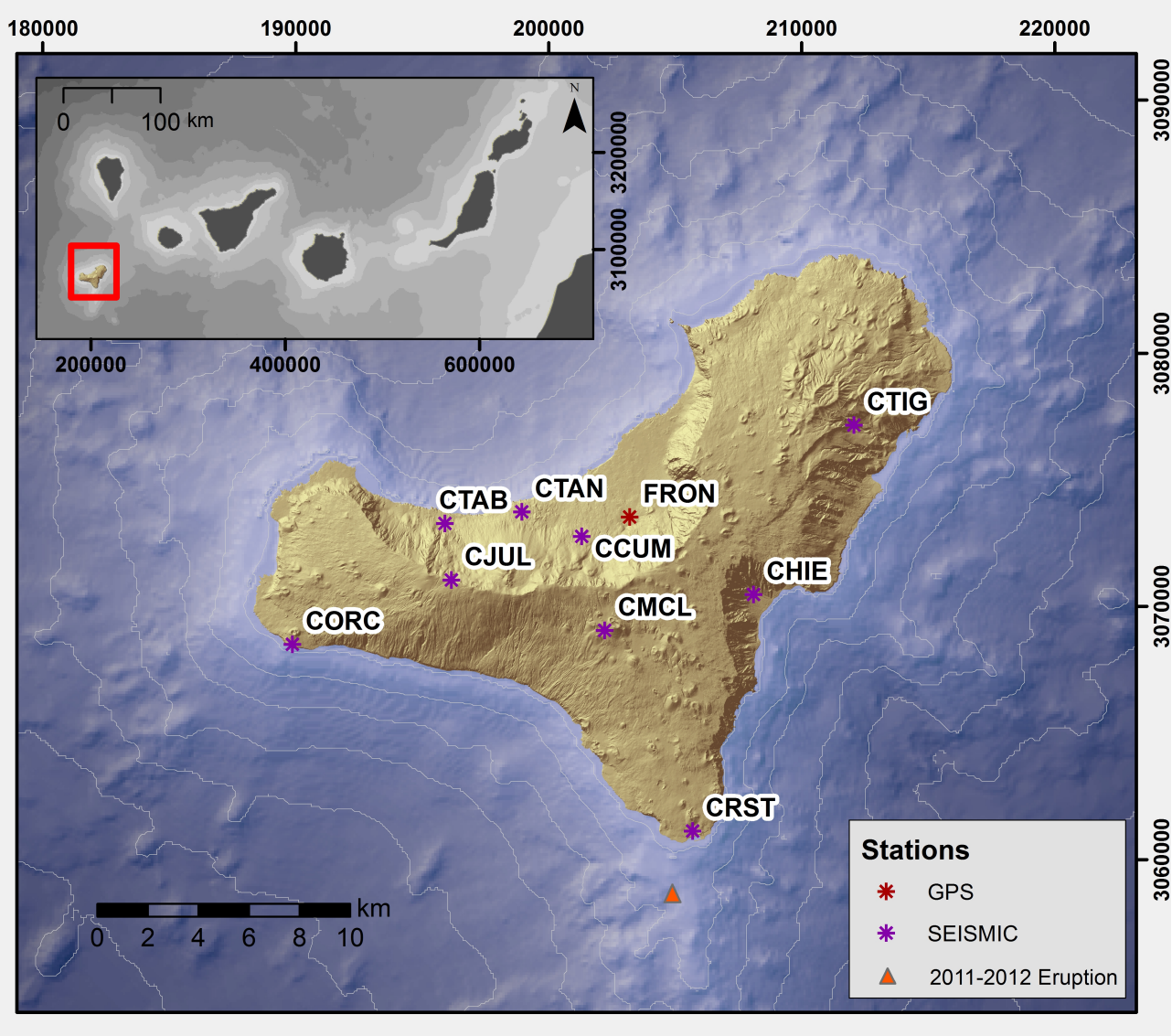
180000
190000
200000
210000
220000
3090000
3080000
3070000
3060000
0
100 km
N
200000
400000
600000
3200000
3100000
CTIG
CTAB
CTAN
FRON
CJUL
CCUM
CHIE
CMCL
CORC
CRST
km
0 2 4 6 8 10
Stations
GPS
SEISMIC
2011-2012 Eruption

Figure 2

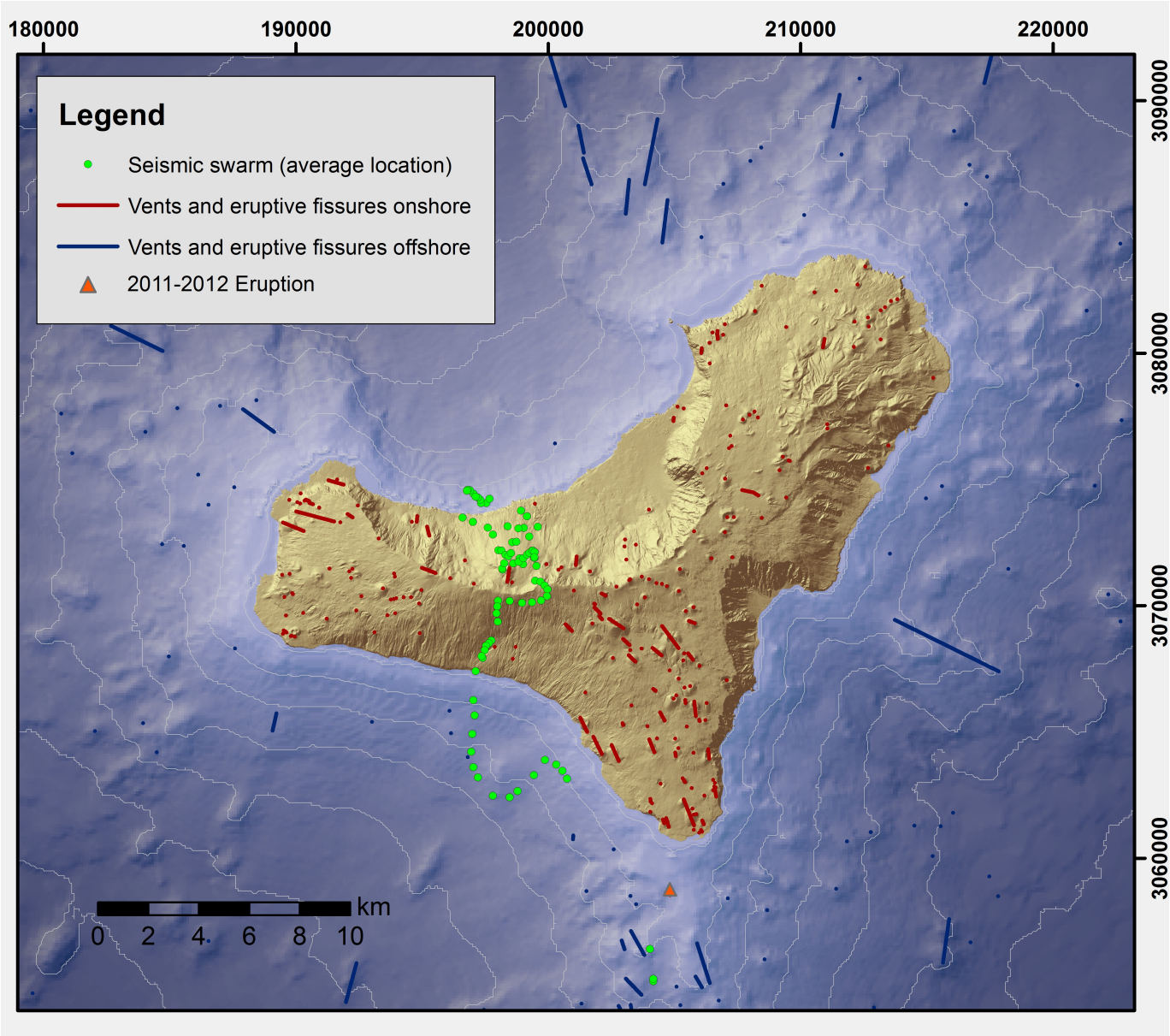
180000
190000
200000
210000
220000
3090000
3080000
3070000
3060000
Legend
Seismic swarm (average location)
Vents and eruptive fissures onshore
Vents and eruptive fissures offshore
2011-2012 Eruption
km
0 2 4 6 8 10

Figure 3

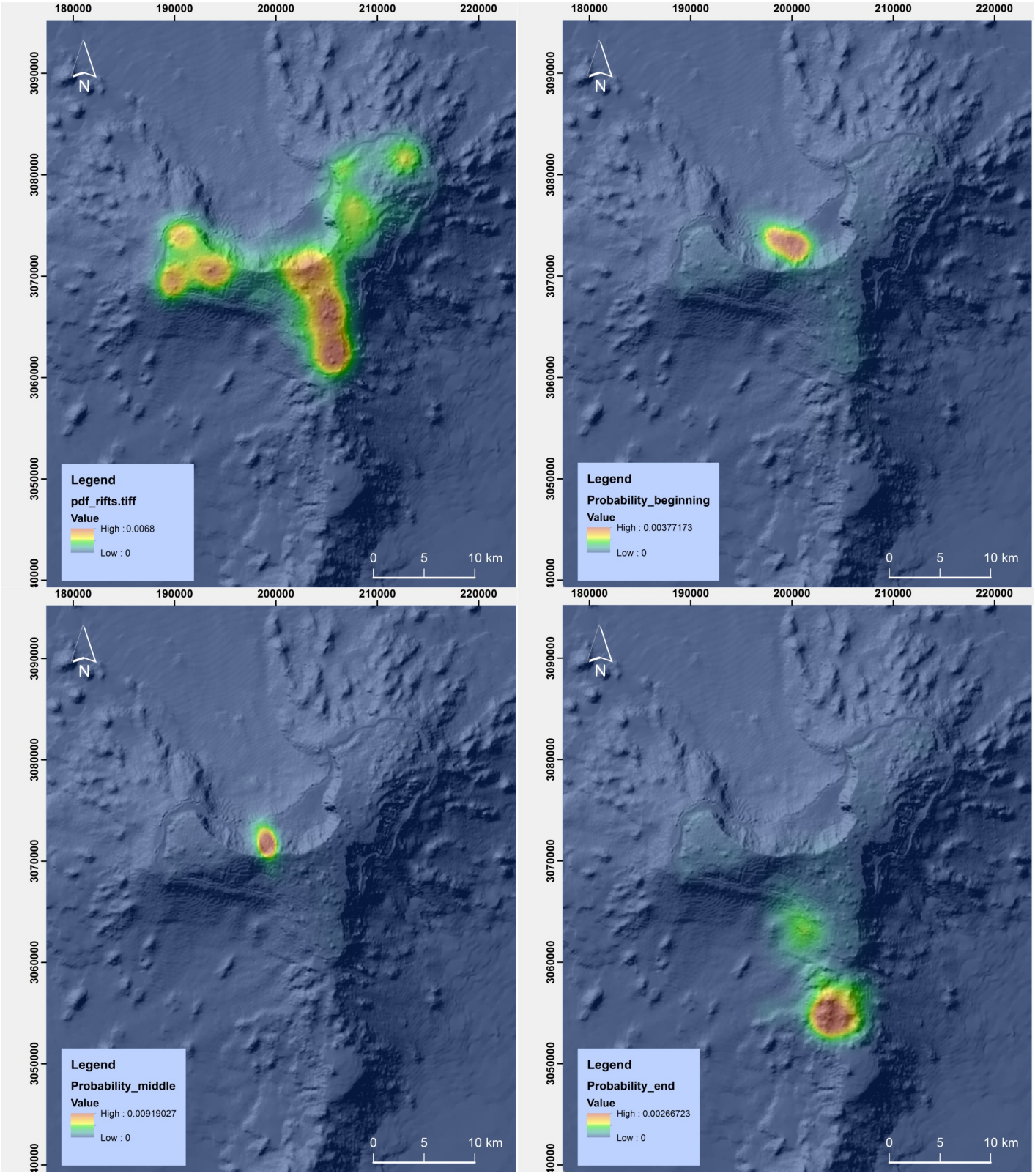
180000
190000
200000
210000
220000
3090000
3080000
3070000
3060000
3050000
40000
N
Legend
pdf_rifts.tiff
Value
High : 0.0068
Low : 0
0
5
10 km
Legend
Probability_beginning
Value
High : 0,00377173
Low : 0
Legend
Probability_middle
Value
High : 0.00919027
Low : 0
Legend
Probability_end
Value
High : 0.00266723
Low : 0

Figure 4

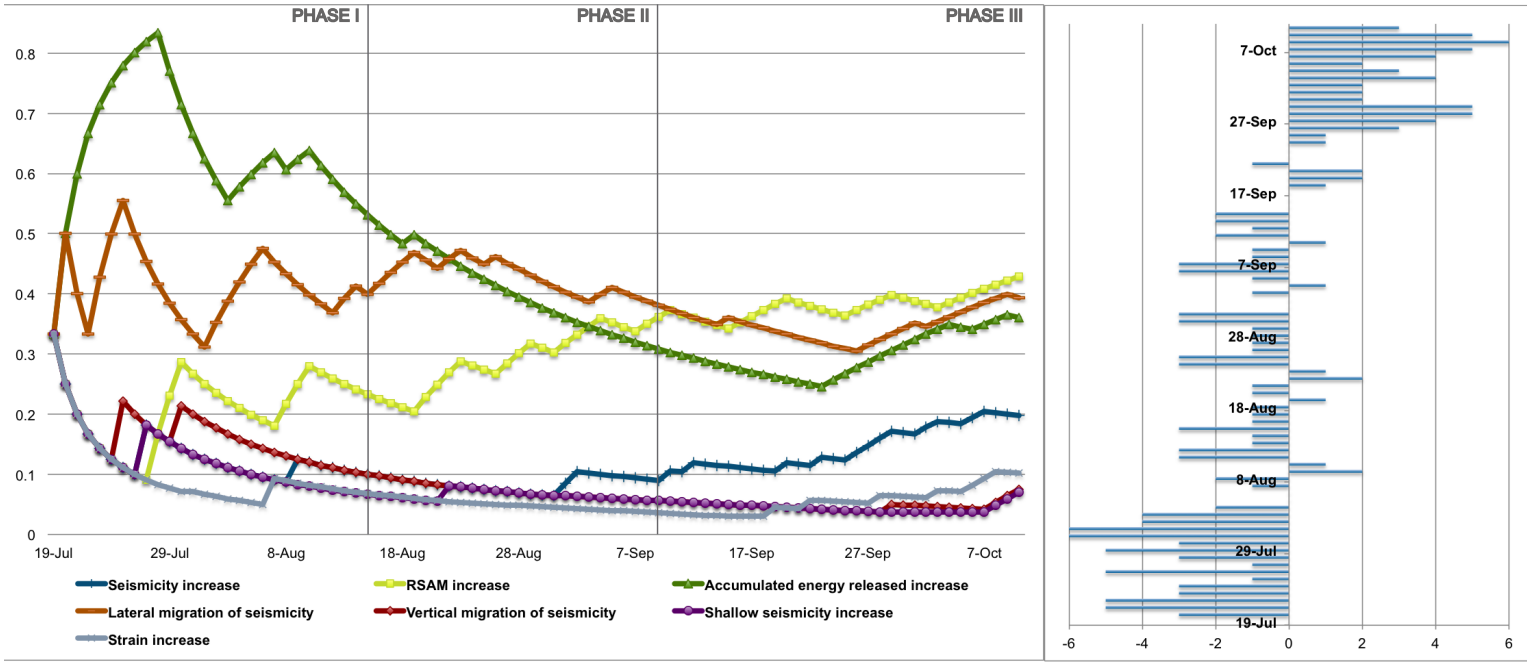
PHASE I
PHASE II
PHASE III
0.8
0.7
0.6
0.5
0.4
0.3
0.2
0.1
0
19-Jul
29-Jul
8-Aug
18-Aug
28-Aug
7-Sep
17-Sep
27-Sep
7-Oct
Seismicity increase
RSAM increase
Accumulated energy released increase
Lateral migration of seismicity
Vertical migration of seismicity
Shallow seismicity increase
Strain increase
7-Oct
27-Sep
17-Sep
7-Sep
28-Aug
18-Aug
8-Aug
29-Jul
19-Jul
-6
-4
-2
0
2
4
6

Figure 5

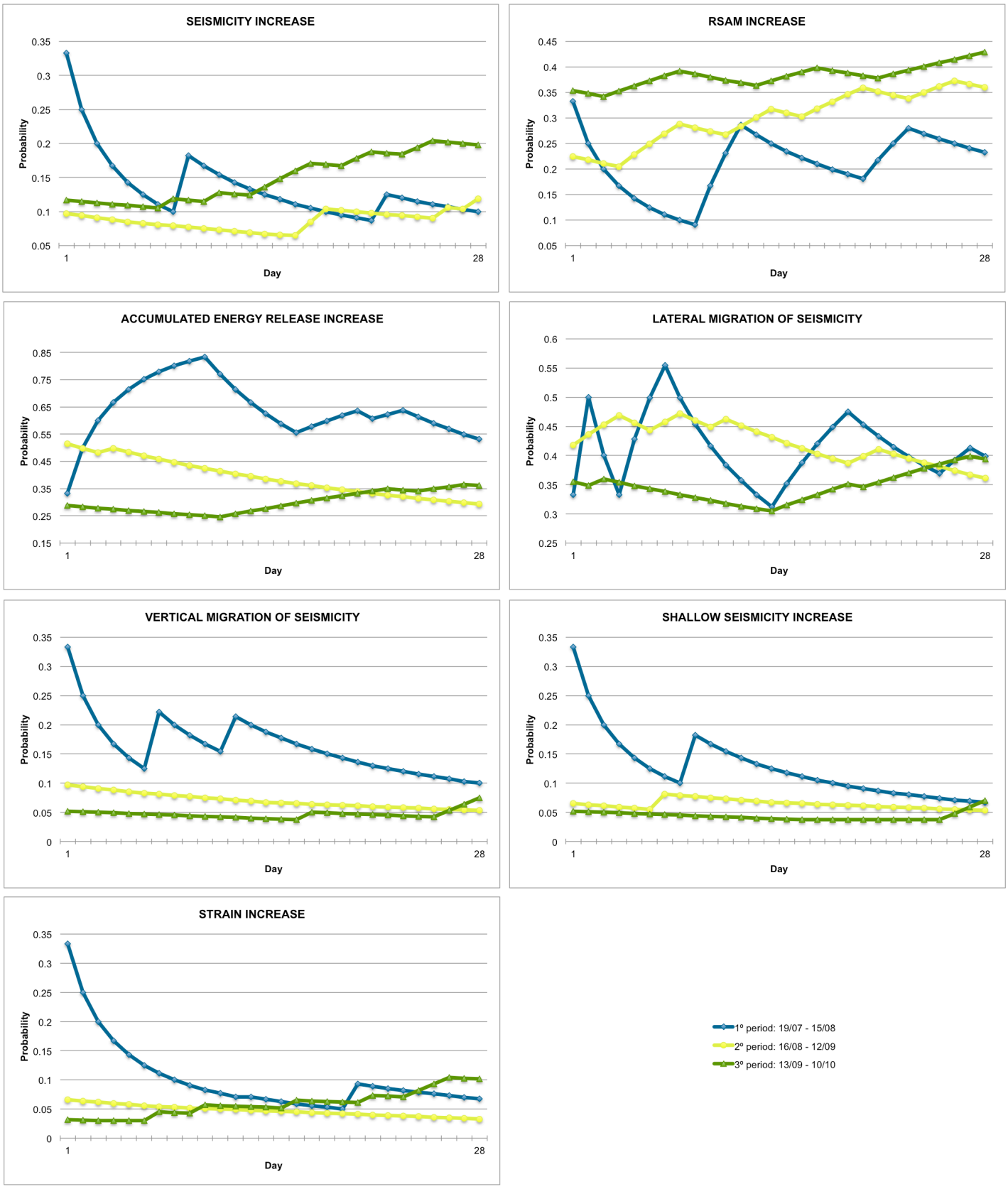
SEISMICITY INCREASE
RSAM INCREASE
ACCUMULATED ENERGY RELEASE INCREASE
LATERAL MIGRATION OF SEISMICITY
VERTICAL MIGRATION OF SEISMICITY
SHALLOW SEISMICITY INCREASE
STRAIN INCREASE
Probability
Day
1
28
1º period: 19/07 - 15/08
2º period: 16/08 - 12/09
3º period: 13/09 - 10/10